Scientia Iranica, Vol. 11, Nos. 1&2, pp 81–91

SCIENTIA
IRANICA

Modeling Heat and Mass Transfer in Falling Film Absorption Generators

S. Jani[1], M.H. Saidi[*], A.A. Mozaffari[1] and A. Heydari[1]

In this paper, heat and mass transfer phenomena occurring simultaneously in falling film generator of absorption chillers have been studied. The analysis is based on the laminar flow of an Li/Br solution over a horizontal single tube and tube bundle having a constant tube wall temperature. The effect of boiling has been ignored. An extensive numerical code is provided to calculate the heat transfer coefficient and the rate of evaporation. A parametric study is performed on the coefficient of heat transfer and the evaporation flux of the refrigerant. Dimensionless correlations are obtained to calculate the heat transfer coefficient on the horizontal tube and tube bundle. The comparison between numerical and analytical results with the existing numerical and experimental data verify the validation of the present model.

INTRODUCTION

Two common designs of absorption generator are, namely, pool boiling and falling film. Falling film generators are more frequently used in absorption chillers. Their operation is based on heat addition through warm/hot water or steam to the Li/Br solution, causing water to boil off from the Li/Br solution. Consequently, there will be a rich solution of Li/Br. Following are the advantages of falling film generators:

a) The heat transfer coefficient is highly enhanced at low temperature differences;
b) The pressure drop inside the generator is minimized as the hydrodynamic driving force is only the gravitational force and no extra pumping is necessary;
c) Due to low static pressure inside the generator, the corresponding saturation temperature is low enough;
d) The volume of Li/Br solution existing in this type of absorption generator is very low.

All the above-mentioned points tend to increase the heat transfer coefficient and decrease the necessary superheat temperature and possibility of using low-grade energy. The majority of experimental and analytical studies on falling film evaporation are based on pure water. Little data are available for the evaporation of Li/Br solution on either horizontal single tubes or tube bundles.

The hydrodynamics of liquid falling film on a horizontal tube consist of three zones, namely, stagnation, impingement and a developed zone, as shown in Figure 1. Miyazaki et al. [1] studied the impingement of falling film jet on horizontal surfaces. They have, theoretically, analyzed the fluid flow and heat transfer of a laminar jet, normal to a heated horizontal plate. Water and compressed air were used as the working fluid. Anberge [2] analytically studied the developing

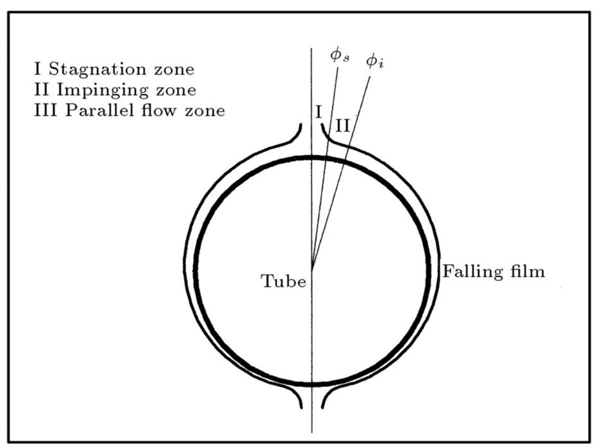

Figure 1. Zoning of the fluid flow on the tube.

1. *Department of Mechanical Engineering, Sharif University of Technology, Tehran, I.R. Iran.*
*. *Corresponding Author, Department of Mechanical Engineering, Sharif University of Technology, Tehran, I.R. Iran.*

and developed hydrodynamic regions for the absorption chamber of the chiller. Mitrovich et al. [3,4] and Jacobi [5] both have studied flow patterns existing in the horizontal tube spacing.

Chyu and Bergles [5] performed experimental and analytical research on a falling film test rig, focusing only on the heat transfer effects. They considered water in a saturated state, neglecting the existence of boiling. They considered two methods to predict their results. The first method was the application of the Nusselt theory, considering only conduction heat transfer in the developing region and the second was adaptation of vertical wall correlations for horizontal tubes. The conclusion was reached that the Nusselt model yields insufficient accuracy on the heat transfer prediction of horizontal tubes. Fletcher et al. [6-8] made an extensive experimental study on the heat transfer phenomena for pure water and seawater in a saturated state over horizontal tubes, considering simultaneous single phase and two phase effects. Turbulent flow with a constant heat flux at the wall was considered and an increased heat transfer coefficient, with an increase in water flow rate, saturation temperature and heat flux, was observed. Lorent and Yang [9] compared the heat transfer coefficient for the falling film of pure water on a single tube and a tube bundle as well. It was concluded that for Reynolds numbers greater than 300, the mean heat transfer coefficient of a tube bundle was the same as for a single tube and the tube arrangement did not affect the heat transfer coefficient. Chen et al. [10,11] focused on the design criteria of falling film evaporators having horizontal tubes. The single tube and tube bundle were regarded and the effects of various factors, such as convective effects, tube diameter, film flow rate and tube spacing, on the heat transfer rate, were considered. Wang et al. [12] introduced a mathematical model of a falling film generator and compared the results with the experimental data achieved from a generator with eight rows of horizontal tubes. It was concluded that as the generator pressure and solution concentration at the inlet decreases, the heat transfer coefficient on the tube wall and the difference between the inlet/outlet Li/Br solution concentration will increase. Also, as the flow rate of weak solution increases, the heat transfer coefficient on the tube wall will increase, while the difference between the inlet/outlet Li/Br solution concentration will decrease. Recently, Kim et al. [13] have studied, experimentally and numerically, a falling film Li/Br solution over a single tube. The heat transfer coefficient for different surface geometries of a horizontal tube was measured and the numerical and experimental results are in fairly good agreement.

In the present study, the objective is to model, numerically, the heat and mass transfer of an Li/ Br solution falling on a horizontal tube and tube bundle. The thermal hydraulic analysis has been performed considering laminar flow and constant tube wall temperature. The effect of boiling has been ignored. The role of liquid impingement on the tube and liquid sheet evaporation in vertical tube spacing and, in the case of a tube bundle, on heat and mass transfer, has been analyzed. The numerical results are compared with the existing analytical and experimental data.

FLUID DYNAMICS

The jet of flow is considered to be divided in two equal parts, as it impinges the upper part of the tube. Three zones can be characterized over the tube surface [1,2], as shown in Figure 1. Flow in the first zone is called the stagnation zone, where the jet flow impinges the upper part of the tube, which is assumed to be isentropic. In the second zone, namely, the impingement zone, a hydrodynamic boundary layer and, subsequently, a viscous sub-layer on the tube surface, will be formed. Since stagnation and impingement zones are very small compared to overall tube perimeter, the flow may be modeled as the impingement of a slot jet on a horizontal surface [5]. A boundary layer penetrates all over the film thickness at the third zone.

The velocity of the mainstream at the first two zones can be derived as:

$$\frac{x}{\delta_s}=\frac{1}{\pi}\left[\ln\left\{\frac{1+u_{\max}/u_j}{1-u_{\max}/u_j}\right\}+\tan^{-1}\left\{\frac{2u_{\max}/u_j}{1-(u_{\max}/u_j)^2}\right\}\right]. \tag{1}$$

In the stagnation zone, velocity increases linearly from the stagnation point [1,5]. The domain of variations of the stagnation zone is restricted by:

$$0<\frac{x}{\delta_s}<0.6 \quad \Rightarrow \quad \varphi_s=0.6(\frac{\delta_s}{R}), \tag{2}$$

$$\delta_s=\frac{2\Gamma}{u_j\rho}, \qquad u_j=\sqrt{2gd_s}. \tag{3}$$

Accordingly, the domain of variations of the impingement zone is written as:

$$0.6<\frac{x}{\delta_s}<2 \quad \Rightarrow \quad \varphi_i=2(\frac{\delta_s}{R}). \tag{4}$$

The Reynolds number in this zone is defined in terms of the velocity outside the boundary layer as:

$$\mathrm{Re}_x=\frac{xu_{\max}(x)}{\nu}. \tag{5}$$

The critical Reynolds number is taken as 4.5×10^5, where the boundary layer shifts from laminar to turbulent.

At the end of the impingement zone, the falling film flow will be fully developed and viscous and body forces are dominating so that the effects of other forces are ignored. Assuming constant property conditions, one can get:

$$u = \frac{\rho g}{\mu} \sin(\varphi)\delta^2 \left[\eta - \frac{\eta^2}{2}\right]. \tag{6}$$

Following is the velocity component, normal to the surface and film thickness, which is obtained by applying the continuity equation:

$$\nu = -\frac{g}{2\nu}\delta^2\eta^2 \left[\frac{1}{s}\frac{d\delta}{d\xi}\sin(\varphi) + \frac{\delta}{R}(1-\frac{\eta}{3})\cos(\varphi)\right], \tag{7}$$

$$\delta = \left[\frac{3\mu\Gamma}{\rho^2 g \sin(\varphi)}\right]^{\frac{1}{3}}. \tag{8}$$

HEAT AND MASS TRANSFER

The falling film of the Li/Br solution at the free surface is assumed to be saturated and the zoning of heat and mass transfer may be considered as in Figure 2. The first zone is the stagnation zone, the second zone is the impingement zone and the third zone is concerned with the formation and penetration of the thermal boundary layer in the film thickness. It is assumed that there is no mass transfer in the three above-mentioned zones and the heat transferred is devoted to the superheating of the Li/Br solution. The fourth zone contains the thermal boundary layer penetrated in the whole thickness of the flow and the formation of a concentration boundary layer. The fourth zone of the tube is important from the point of view of refrigerant generation. In this zone, as the concentration of Li/ Br solution gradually increases, the saturation temperature of the free surface will be increased.

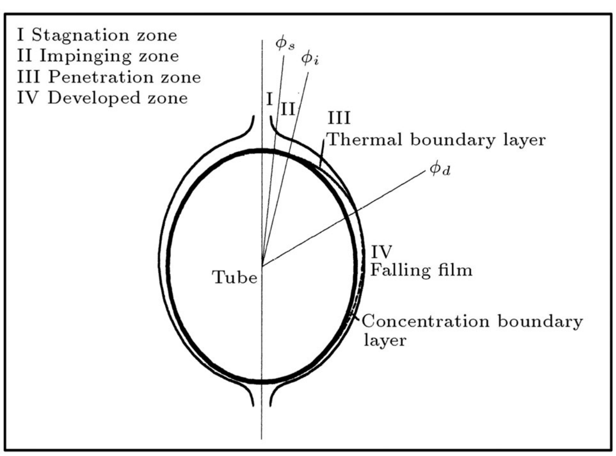

Figure 2. Zoning of the heat transfer.

Analysis of Heat Transfer in Stagnation and Impingement Zones

In these two zones, the quantity of the heat transfer coefficient is equal to [5]:

$$h_s = 1.03\,\mathrm{Pr}^{1/3}\,k\left[\frac{\pi}{4}\times\frac{u_j}{\nu\delta_s}\right]^{0.5}, \tag{9}$$

$$\frac{h_i x}{k} = 0.73\,\mathrm{Pr}^{1/3}\,\mathrm{Re}_x^{0.5}, \tag{10}$$

$$\frac{h_i x}{k} = 0.037\,\mathrm{Pr}^{1/3}\,\mathrm{Re}_x^{0.8}. \tag{11}$$

In which Correlations 10 and 11 are used for the laminar and turbulent boundary layer, respectively.

Analysis of Heat Transfer in the Thermal Boundary Layer Zone

In this zone, the hydrodynamic profile is fully developed and viscous effects have penetrated in the thickness of the falling film. Heat transfer from the tube wall to the flowing Li/Br solution causes the solution to become superheated. The integral equations are used for determining the temperature profile, the heat transfer coefficient and the angle of penetration of the thermal boundary layer in the film thickness. These equations are written as follows:

$$\rho c_p \frac{d}{dx}\int_0^{\Delta} u(T-T_i)dy = -k(\frac{\partial T}{\partial y})_{y=0}. \tag{12}$$

Boundary conditions for temperature profile consist of:

$$T(0,y) = T_i, \qquad T(x,0) = T_w,$$

$$T(x,\Delta) = T_i, \qquad \frac{\partial T(x,\Delta)}{\partial y} = 0. \tag{13}$$

The dimensionless temperature profile is considered as a quadratic profile:

$$\frac{T-T_w}{T_i-T_w} = 2\zeta - \zeta^2. \tag{14}$$

Substituting the temperature profile in Equation 12 and simplifying, results in:

$$\frac{1}{9}\zeta^3 - \frac{1}{40}\zeta^4 = \frac{4\alpha R}{3}\left[\frac{3\mu\Gamma^4}{g\rho^5}\right]^{-1/3}\int_0^{\varphi}[\sin(\varphi')]^{1/3}\,d\varphi'. \tag{15}$$

The average heat flux can be defined as:

$$\overline{q}''_{d,(0-\varphi)} = \frac{1}{x}\int_0^x (-k\frac{\partial T(x,y)}{\partial y})_{y=0}\,dx$$

$$= \frac{2k(T_w-T_i)}{x}\int_0^x \frac{dx}{\Delta}. \tag{16}$$

The average heat transfer coefficient can be written as:

$$\overline{h}_{d,(0-\varphi)} = \frac{\overline{q}''_{d,(0-\varphi)}}{(T_w - T_i)} = \frac{2k}{x}\int_0^x \frac{dx}{\Delta}. \qquad (17)$$

The end of this zone is characterized by a value of $\zeta = 1$, where the thermal boundary layer has penetrated the whole thickness of the falling film. Therefore, substituting $\zeta = 1$ in Equation 15, one can write:

$$T(\varphi) = \int_0^\varphi [\sin(\varphi')]^{1/3}\, d\varphi' = \frac{31}{480}\frac{1}{\alpha R}\left[\frac{3\mu_{\Gamma^4}}{g\rho^5}\right]^{1/3}. \qquad (18)$$

A linear approximation of T(φ) will result in:

$$T(\varphi) = 0.83667\varphi.$$

So that the angle of penetration depth can be expressed as:

$$\varphi_d = 0.07751\frac{1}{\alpha R}\left[\frac{3\mu_{\Gamma^4}}{g\rho^5}\right]^{1/3}. \qquad (19)$$

Lorenz and Yang [9] have reached the following correlation in their research for the angle of penetration depth:

$$\varphi_d = 0.07958\frac{1}{\alpha R}\left[\frac{3\mu_{\Gamma^4}}{g\rho^5}\right]^{1/3}. \qquad (20)$$

Chyu and Bergles [5] defined the angle of penetration depth at a point where the temperature profile tends to become linear. The following correlation was discovered:

$$\varphi_d = 0.31831\frac{1}{\alpha R}\left[\frac{3\mu_{\Gamma^4}}{g\rho^5}\right]^{1/3}. \qquad (21)$$

Heat and Mass Transfer in Thermal Developed Zone and Concentration Boundary Layer

In this zone, the thermal profile is developed in the all over falling film thickness and the concentration boundary layer is growing. The differential forms of mass and energy conservation in dimensionless forms consist of:

$$\frac{u}{s}\frac{\partial\theta}{\partial\xi} + \left(\frac{\nu}{\delta} - \frac{\eta}{\delta}\frac{d\delta}{d\xi}\frac{u}{s}\right)\frac{\partial\theta}{\partial\eta} = \frac{\alpha}{\delta^2}\frac{\partial^2\theta}{\partial\eta^2},$$

$$\frac{u}{s}\frac{\partial w}{\partial\xi} + (\frac{\nu}{\delta} - \frac{\eta}{\delta}\frac{d\delta}{d\xi}\frac{u}{s})\frac{\partial w}{\partial\eta} = \frac{D}{\delta^2}\frac{\partial^2 w}{\partial\eta^2}. \qquad (22)$$

The initial and boundary conditions can be written as:

$$\begin{array}{ll}
\theta = (T_s - T_w)(2(\eta) - (\eta)^2) & \xi = \xi_i,\ 0 \le \eta \le 1 \\
w = w_i & \xi = \xi_i,\ 0 \le \eta \le 1 \\
\theta = 0 & \eta = 0,\ \xi_i \le \xi \le \xi_e \\
\frac{\partial w}{\partial\eta} = 0 & \eta = 0, \xi_i \le \xi \le \xi_e \\
\theta = \theta_s = f(P, w_s) & \eta = 1, \xi_i \le \xi \le \xi_e \\
M'' = \frac{\rho D}{w_s\delta}\frac{\partial w}{\partial\eta} = \frac{q''}{h_{fg}} = -\frac{k}{h_{fg}\delta}\frac{\partial\theta}{\partial\eta} & \eta = 1, \xi_i \le \xi \le \xi_e
\end{array} \qquad (23)$$

Velocity components u and ν and the thickness of falling film are estimated from Correlations 6 to 8. One may realize the set of differential Equations 22 as of the parabolic type. These sets of equations have coupled boundary conditions and variable coefficients as well. In the absence of any clear analytical solution, a numerical method is used to solve them. The Crank-Nicolson implicit method is used for solving conservation equations. A finite difference scheme, having a forward difference in ξ direction and an averaged central difference in η direction, are used. It is shown that the final round off error of discrete equations has the order of $O(\Delta\xi^2, \Delta\eta^2)$.

The local heat transfer coefficient can be obtained from the following correlation:

$$h_\varphi = \frac{-k\frac{\partial\theta}{\partial y}\Big|_{y=0}}{T_w - T_i} = \frac{\frac{-k}{\delta}\frac{\partial\theta}{\partial\eta}\Big|_{\eta=0}}{-\theta_i} = \frac{k}{\delta\theta_i}\frac{\partial\theta}{\partial\eta}\Big|_{\eta=0}. \qquad (24)$$

Total Mean Heat Transfer Coefficient on the Tube

The total mean heat transfer coefficient on the tube is composed of the sum of the weighted heat transfer coefficients obtained in each zone [5]. Therefore:

$$\overline{h}_{\text{tot}} = \overline{h}_s\left(\frac{\varphi_s}{\pi}\right) + \overline{h}_i\left(\frac{\varphi_i - \varphi_s}{\pi}\right) + \overline{h}_d\left(\frac{\varphi_d - \varphi_i}{\pi}\right) + \overline{h}_{fd}\left(1 - \frac{\varphi_d}{\pi}\right). \qquad (25)$$

TUBE BUNDLE

Thermal hydraulic analysis of a tube bundle consists of: (a) Heat and mass transfer over the horizontal tubes, (b) Heat and mass transfer in a liquid sheet of vertical tube spacing; and (c) Impingement region at the top of the tubes. These three regions must be simultaneously solved to obtain the heat and mass transfer characteristics of the tube bundle. The falling film will be heated and concentrated, while flowing over the tube. The superheat temperature of the falling film, while passing through tube spacing, will be decreased and, simultaneously, will be concentrated. The dimensionless parameters for the tube bundle are defined, based on local physical properties, on the top of each tube. The results of a single tube have been generalized for a tube bundle, neglecting end effects and column interaction. In order to specify the temperature and concentration profiles in the liquid sheet at tube spacing, bulk and surface temperature and concentration, must be evaluated. It is assumed that the Li/Br solution, once leaving the tube, has no velocity component and the liquid films of two sides of the tube are well mixed. A uniform bulk temperature and concentration of Li/Br solution may be estimated, based on energy and mass conservation, over the tube. This bulk temperature and concentration are used as the initial temperature and concentration for analysis of the liquid sheet at tube spacing. Applying energy and continuity equations for the Li/Br solution, taking into account the corresponding quadratic temperature and concentration profiles, leads to the following set of equations, in which 2Γ and δ_s are mass flow rate and liquid sheet thickness, respectively:

$$\frac{T-T_s}{T_o-T_s}=1-(2y/\delta_s)^2,$$

$$\frac{w-w_s}{w_o-w_s}=1-(2y/\delta_s)^2,$$

$$\frac{d}{dx}(T_m)=\frac{6\rho\alpha}{\Gamma\delta_s}(T_s-T_m),$$

$$\frac{d}{dx}(w_m)=\frac{6\rho D}{\Gamma\delta_s}(w_s-w_m),$$

$$f(T_s,w_s)=0,$$

$$\frac{\rho D}{w_s}(w_m-w_s)h_{fg}=-k(T_m-T_s). \tag{26}$$

This set of nonlinear differential equations has been solved using the fourth Runge-Kutta finite difference method to determine bulk and free surface temperature and concentration at any vertical location in the tube spacing.

Realization of heat and mass transfer mechanisms in the horizontal tube bundle is necessary, in order to derive the relevant governing equations. The Li/Br solution, in a saturated state, falls down on the first row. Heat addition to the liquid occurs from the tube surface, while evaporation takes place at the free surface. Bulk temperature and concentration can be calculated at the lower point of the first tube row, which is used as an initial condition for the vertical liquid sheet at the tube spacing. Evaporation takes place from the vertical liquid sheet at the tube spacing and the bulk temperature of the liquid reduces and approaches saturation temperature. The process of liquid impingement for lower tube rows is the same, having different physical properties and mass flow rate.

RESULTS AND DISCUSSIONS

Results for a single tube and tube bundle are based on the local estimation of thermo physical properties of the Li/Br solution. Discussion of the results for a single tube and tube bundle are given below.

Single Tube

Distribution of the thickness of falling film of an Li/Br solution on the periphery of a horizontal tube is shown in Figure 3. With the exception of the top and bottom of the tube periphery, falling film thickness does not change greatly. The thickness of the thermal boundary layer profiles obtained, based on the numerical and energy integral methods, has been compared in Figure 4.

The results of the present work and the numerical results of Kim et al. [13] are compared in Figures 5 to 8. The discrepancies in the results are mainly due to the discretization order of the mass transfer boundary condition on the free surface. Since the concentration profile near the free surface is not linear, applying the second order discretization method predicts more accurate results. The bulk and free surface temperatures and concentrations of the Li/Br solution are shown in Figures 5 and 6, respectively. Overestimation of

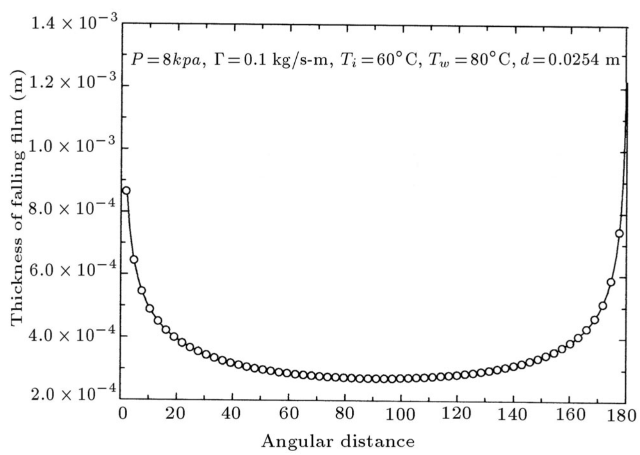

Figure 3. Thickness of falling film vs. angular position.

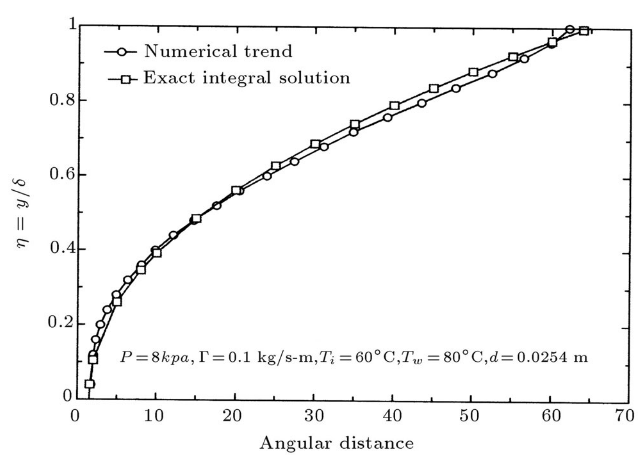

Figure 4. Thermal boundary layer vs. angular position.

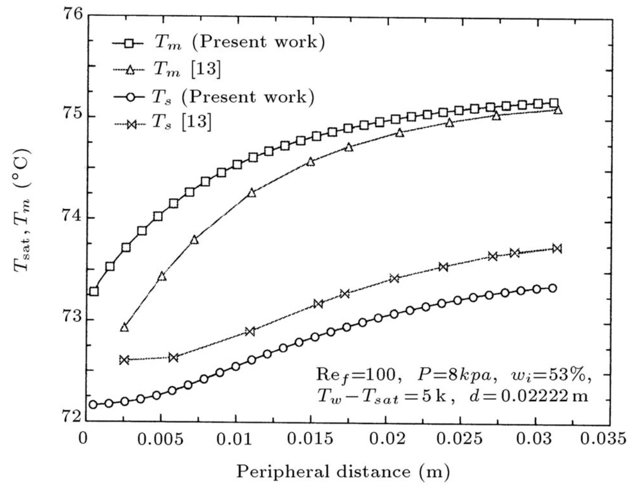

Figure 5. Bulk and free surface temperature vs. peripheral distance.

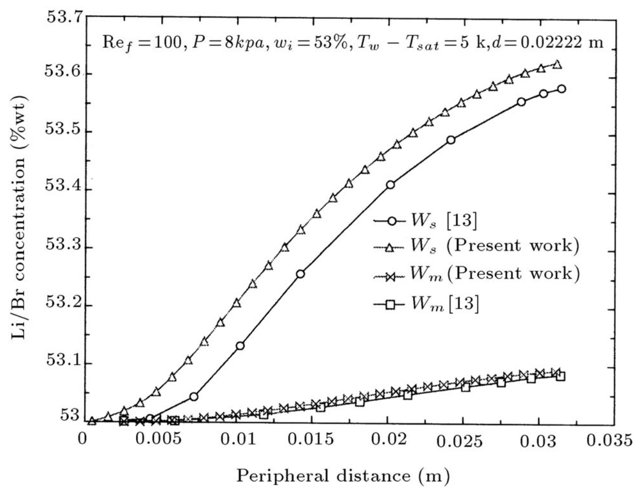

Figure 6. Bulk and free surface concentration vs. peripheral distance.

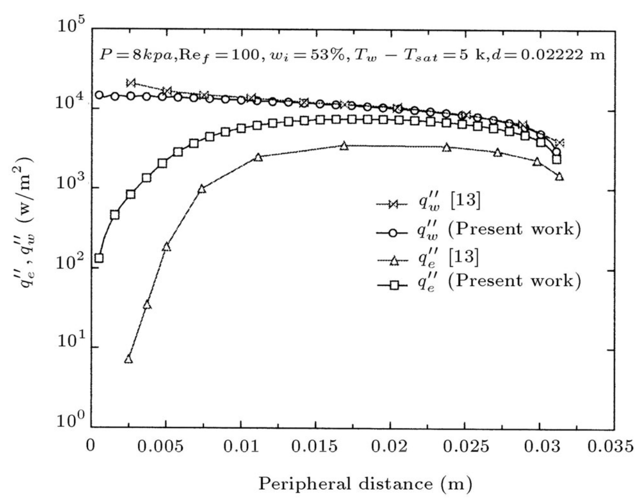

Figure 7. Heat flux at the wall and free surface vs. peripheral distance.

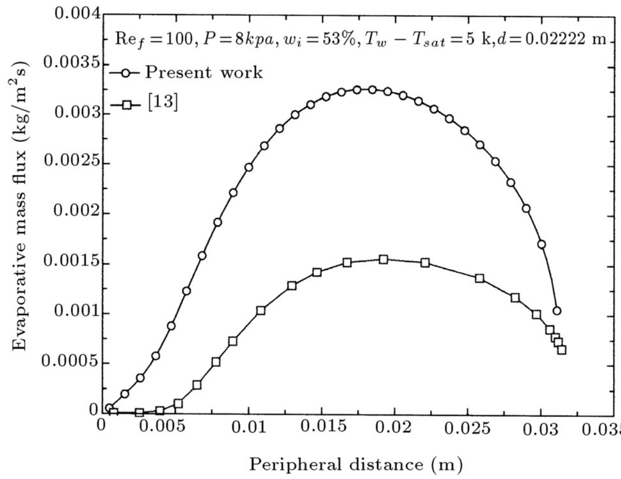

Figure 8. Evaporative mass flux vs. peripheral distance.

the bulk temperature near the upper part of the tube is due to stagnation and impingement heat transfer effects. Simultaneous underestimation of free surface temperature and overestimation of free surface concentration is the consequence of modifications, which is performed for the order of concentration discretization at the free surface. The heat flux distributions at the wall and free surface over the periphery of the tube are given in Figure 7. Net heat, transferred to the falling film of the Li/Br solution over the horizontal tube, is calculated from subtraction of the wall heat flux from the free surface heat flux. The net heat flux is a source of superheat temperature and, subsequently, liquid sheet evaporation in tube spacing. The evaporative mass flux, with respect to tube periphery, is shown in Figure 8 and compared with the existing numerical results [13]. The evaporative mass flux reaches its maximum value at a location having minimum falling film thickness.

The ratio of the average sensible heat to the average total heat flux at the tube wall, as a function of the Reynolds number of falling film, is shown in Figure 9. Average sensible heat flux is defined as the difference between average wall and free surface heat fluxes. At low Reynolds number, the predicted values are in good agreement with the existing experimental data of Kim [13]. However, at high Reynolds number, due to wavy effects at the free surface, the numerical results diverge from experimental data. The numerical and experimental results of average wall heat flux vs. falling film Reynolds number are shown in Figure 10. As seen, wall heat flux increases with increasing Reynolds number. A comparison of average evaporative mass flux over the tube, as a function of wall superheat, for the present work and the experimental data, is given in Figure 11. Evaporative mass flux increases with increasing wall superheat. Dependency of the average wall heat flux and evaporative mass flux on the system pressure is shown in Figures 12 and 13, respectively.

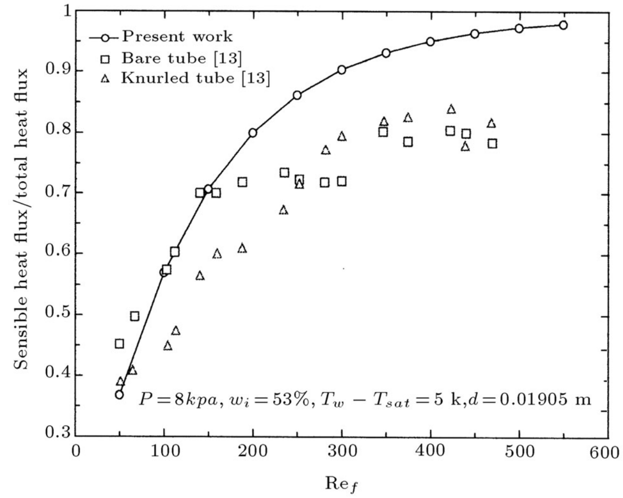

Figure 9. Ratio of sensible heat flux to wall heat flux vs. film Reynolds number.

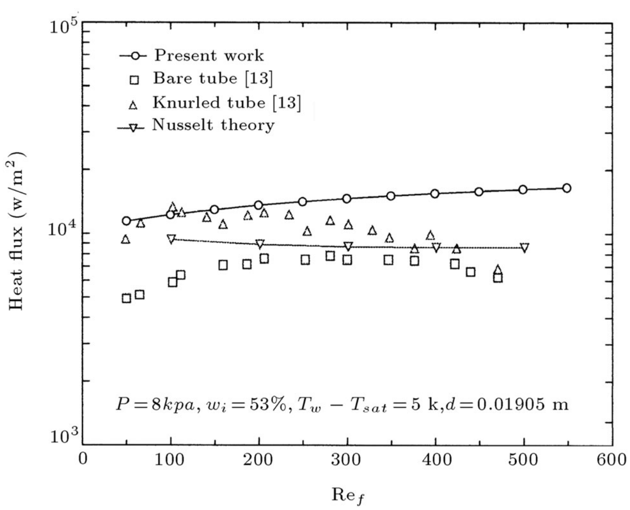

Figure 10. Heat flux at wall surface vs. Reynolds number.

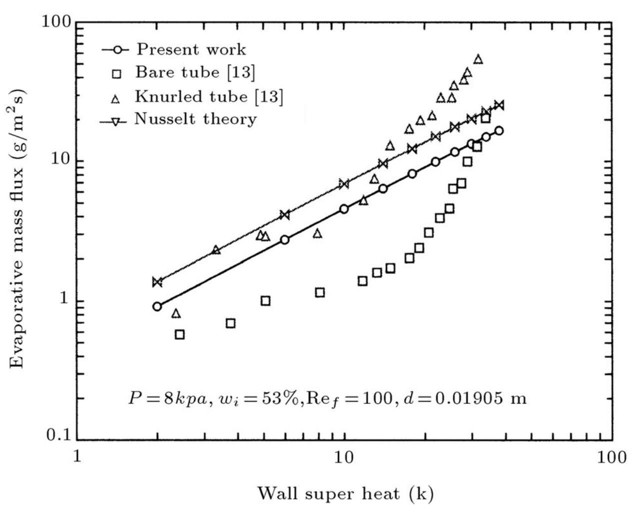

Figure 11. Evaporative mass flux vs. wall superheat.

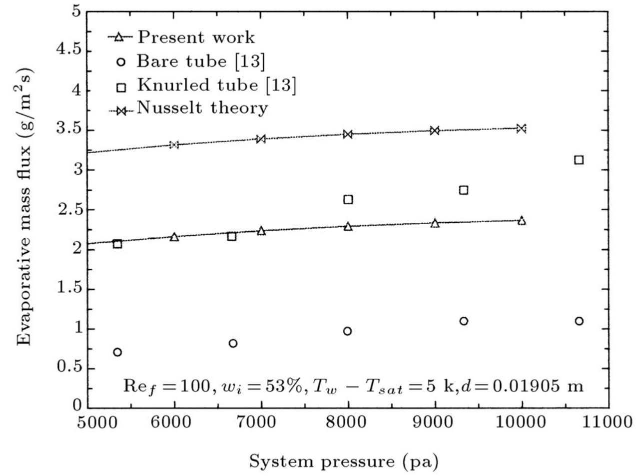

Figure 12. Evaporative mass flux vs. system pressure.

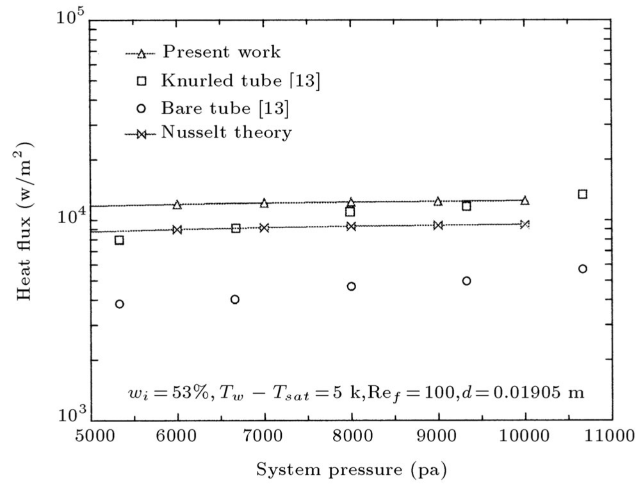

Figure 13. Total heat flux vs. system pressure.

Evaporative mass flux and wall heat flux increase with increasing system pressure. This is due to the fact that increasing the system pressure tends to increase the saturation temperature and decrease the viscosity of the solution. Furthermore, this causes falling film thickness to decrease and wall heat to increase flux. The outcome of this trend is an increase in evaporative mass flux. Figures 14 and 15 show the behavior of the heat transfer coefficient and evaporative mass flux vs. the inlet Li/Br concentration, respectively. The thickness of falling film increases with increasing inlet concentration, while the wall heat transfer coefficient and evaporative mass flux decrease.

The general dimensionless form of heat transfer coefficient for the falling film on a tube is given by:

$$\frac{\overline{h}L_c}{k} = a_1 \mathrm{Re}_f^{a}2\,\mathrm{Pr}^{a_3}\,p^{a_4} e^{a_5 w}, \quad L_c = \left(\frac{\mu^2}{\rho^2 g}\right)^{\frac{1}{3}}. \qquad (27)$$

Applying logarithmic regression of the present numerical data of the Li/Br solution, considering Correlation 27, one will obtain the following general correlation

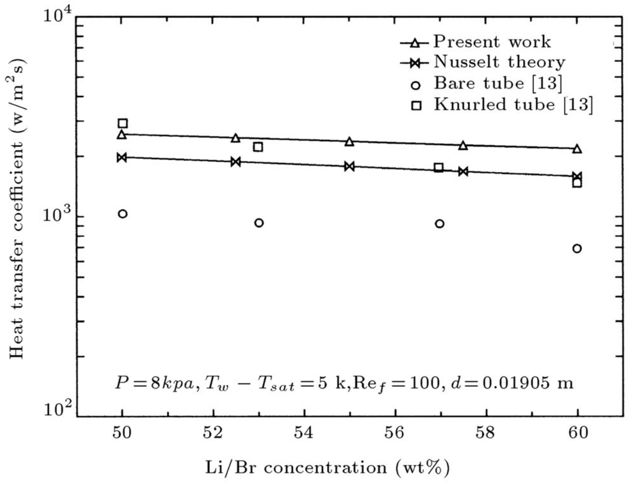

Figure 14. Heat transfer coefficient vs. Li/Br concentration.

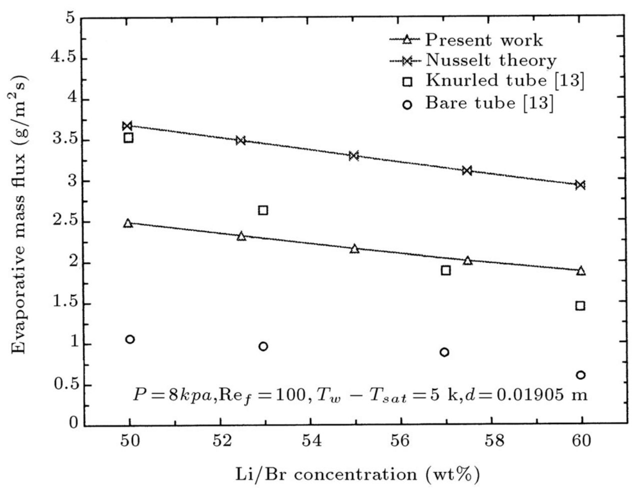

Figure 15. Evaporative mass flux vs. Li/Br concentration.

of heat transfer coefficient for the falling film of the Li/Br solution over a single horizontal tube:

$$\frac{\overline{h}L_c}{k}=0.02374\times\mathrm{Re}_f^{0.1957}\,\mathrm{Pr}^{0.7662}\,P^{0.03643}e^{-0.00618\times w}. \tag{28}$$

It should be noted that the thermodynamic properties are calculated at the mean of the saturated temperature of the Li/Br solution and wall temperature. The domain of applicability of Correlation 28 are specified below:

$$7<\mathrm{Pr}<10,$$

$$100<\mathrm{Re}_f<500,$$

$$5.5\ kpa<P<10.5\ kpa,$$

$$50\%<w<60\%. \tag{29}$$

Correlation 28 has a maximum error of about 1%, compared to the numerical solution.

Tube Bundle

A tube bundle composed of 20 rows has been considered and parametric study has been performed, based on generalization of single tube behavior and taking into account the evaporation of the liquid sheet at tube spacing. Figure 16 shows variations of heat transfer coefficient vs. number of tube rows for different tube diameters. The heat transfer coefficient decreases as the tube diameter increases. Also, the highest heat transfer coefficient is found to be at the first tube row and decreases gradually in the subsequent tube rows, with a final approach of a constant value, once the number of tube rows tends to become infinite. Figure 17 shows heat transfer coefficient vs. number

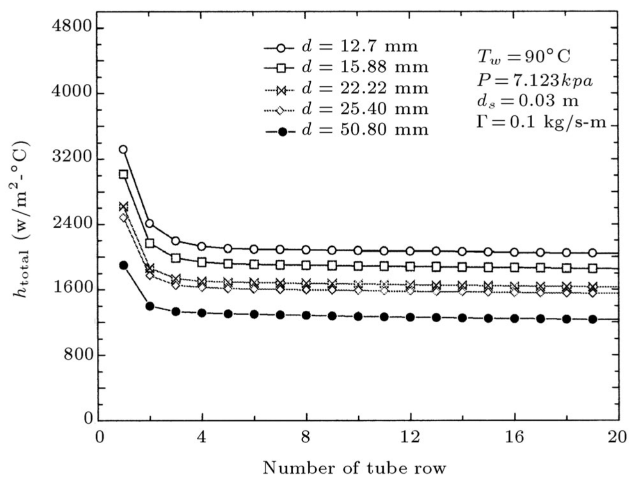

Figure 16. Heat transfer coefficient in the tube bundle vs. tube diameter.

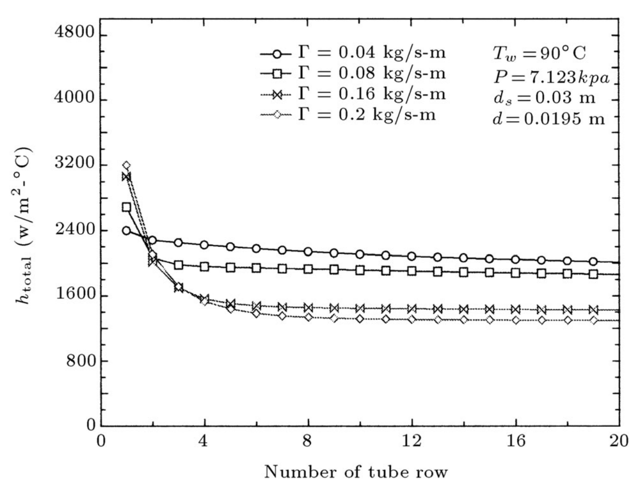

Figure 17. Heat transfer coefficient in the tube bundle vs. mass flow rate.

of tube rows for different mass flow rates. As the mass flow rate of Li/Br is increased the heat transfer coefficient decreases. Figure 18 shows the heat transfer coefficient vs. number of tube rows for different tube spacings. The heat transfer coefficient increases with increasing tube spacing. Heat transfer coefficient and system pressure are dependent, according to Figure 19. Similar to a single tube, the heat transfer coefficient increases with increasing system pressure. The results show that the heat transfer behavior of the tube bundle can be simulated as the behavior of flow inside a horizontal tube. This is verified by the experimental work of Kocamustafaogullari et al. [11]. Hence, the tube bundle can be divided into two zones, namely, entrance zone and steady state zone. The heat transfer coefficient at the entrance zone is a function of the number of tube rows, while the heat transfer coefficient is nearly constant in the steady state zone.

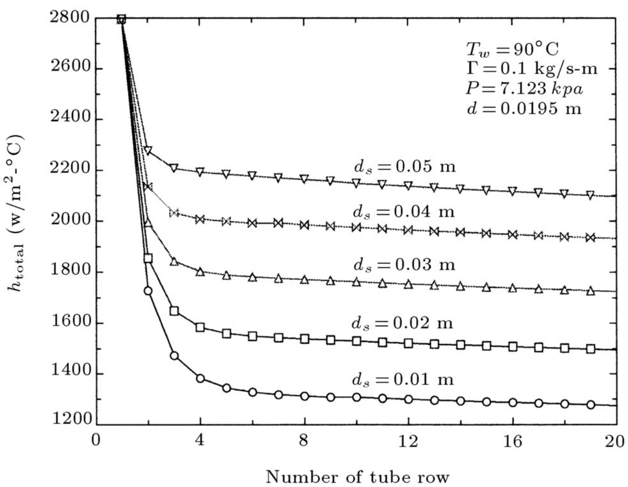

Figure 18. Variation of heat transfer coefficient in the tube bundle vs. tube spacing.

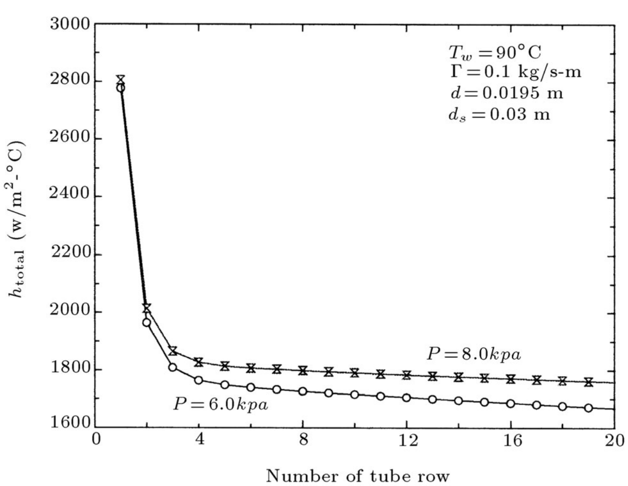

Figure 19. Variation of heat transfer coefficient in the tube bundle vs. system pressure.

The number of tube rows, in which the transition from entrance to steady state takes place, is given by:

$$Nc = E(7.4204 + 0.015533\,\mathrm{Re}_f - 0.011804\,d^* - 0.0020464\,ds^*). \tag{30}$$

where E is bracket function and Nc is the number of tube rows in which the flow over the tube rows becomes steady state.

The average Nusselt number at the entrance zone can be expressed as:

$$a_0 = 0.90208, \quad a_1 = 0.13333, \quad a_2 = -0.00063985,$$

$$a_3 = -0.31944, \quad a_4 = 0.031683, \quad a_5 = 0.037499,$$

$$a_6 = -0.031278, \quad a_7 = 0.0058041, \quad a_8 = 0.30457,$$

$$\overline{\mathrm{NU}} = a_0 f_n \mathrm{Re}_f^{a_1} e^{a_2 \mathrm{Re}_f} d^{*a_3} ds^{*a_4}\,\mathrm{Pr}^{a_5} P^{a_6} e^{a_7 w}$$

$$f_n = \left(\frac{0.563561 \times n - 0.291792}{2.75364 \times n - 2.38221}\right)^{a_8} \qquad n \geq 2. \tag{31}$$

Subsequently, for the steady state zone, the Nusselt number is given by:

$$a_0 = 0.47628, \quad a_1 = 0.17725, \quad a_2 = -0.001046,$$

$$a_3 = 0.10137, \quad a_4 = 0.26702, \quad a_5 = 0.011055,$$

$$a_6 = 0.000082563,$$

$$\overline{\mathrm{NU}} = a_0 \mathrm{Re}_f^{a_1} e^{a_2 \mathrm{Re}_f}\,\mathrm{Pr}^{a_3}\, d^{*a_4} P^{a_5} e^{a_6 ds^*}. \tag{32}$$

The domain of applicability of the above-mentioned equations is given in Equation 29. Correlations 31 and 32 have a maximum error of about 15%, compared to numerical results.

CONCLUSION

In this research, the thermal behavior of Li/Br falling film absorption generators has been numerically modeled. Investigation has been performed for a horizontal single tube and tube bundle.

The results show that by increasing the Li/Br flow rate, the angle of penetration depth, the heat transfer coefficient on the tube and liquid film thickness will increase, while the total refrigeration produced on a single tube will decrease.

Increasing tube wall temperature will linearly increase both the refrigerant flux of evaporation and the heat flux on the tube wall.

Increasing pressure will increase the saturation temperature of inlet Li/ Br. Subsequently, the viscosity of the solution decreases and causes a reduction in film thickness and an increase in heat and mass flux on the free surface.

Increasing inlet concentration will increase the viscosity of the solution, resulting in an increase in film thickness and a decrease in heat transfer coefficient and mass flux.

The thermal-hydraulic behavior of the tube bundle has been studied, based on the single tube and tube spacing. Present investigations showed that the thermal behavior of the horizontal tube bundle in falling film evaporation is nearly the same as the internal flow and heat transfer in a horizontal tube. With this similarity, the heat transfer coefficient for the first row has reached its maximum and will decrease in the subsequent rows up to the developed region, which tends to become constant and independent of the following rows.

Finally, analytical correlations of the heat transfer coefficient for a single tube and tube bundle are extracted.

NOMENCLATURE

c_p	specific heat at constant pressure
D	diffusion coefficient
d	outer tube diameter
d^*	dimensionless tube diameter (d/L_c)
d_s^*	dimensionless vertical tube spacing (d_s/L_c)
d_s	vertical tube spacing, jet height
g	gravitational constant
h	heat transfer coefficient
h_{fg}	latent heat of evaporation
k	thermal conductivity
L_c	characteristic length $(\nu^2/\mathrm{g})^{1/3}$
M''	evaporation mass flux
N	tube number
Nu	Nusselt number (hLc/k)
P	system pressure
Pr	Prandtl number
q''	heat flux
R	outer tube radius
Re_f	film Reynolds number $(4\Gamma/\mu)$
Re_x	peripheral Reynolds number
s	peripheral distance (πR)
T	temperature
u	peripheral velocity
u_j	jet free velocity
$u_{\max}$	main stream flow velocity
ν	normal flow velocity
x	peripheral length
w	Li/Br concentration
y	normal distance

Greek Symbols

α	thermal diffusion coefficient
δ	falling film thickness
δ_s	liquid sheet thickness, jet width
Δ	thermal boundary layer thickness
Γ	Li/Br solution flow rate per unit length per one side of tube
η	dimensionless vertical distance (y/δ)
φ	angular distance
μ	liquid dynamic viscosity
ν	liquid kinematics viscosity
θ	temperature index
ρ	density
ξ	dimensionless peripheral distance $(x/(\pi.R))$
ζ	dimensionless parameter (y/Δ)

Subscript

d	developing zone
e	exit, evaporation
f_d	fully developed zone
i	impingement zone, initial, inlet
m	mean value
o	center line
p	constant pressure
s	stagnation zone, saturation, free surface
w	tube wall
tot	total

REFERENCES

1. Miyazaki, H. and Silberman, H. "Flow and heat transfer on a flat plate normal to a two-dimensional laminar jet issuing from a nozzle of finite height", *Int. J. Heat and Mass Transfer*, **15**, pp 2097-2107 (1972).

2. Anberg, J.W. "Absorption of vapor into liquid films flowing over cooled horizontal tubes", Ph.D. Thesis, University of Texas at Austin, USA (1986).

3. Armbruster, R. and Mitrovic, J. "Evaporative cooling of a falling water film on horizontal tubes", *Experimental Thermal and Fluid Science*, **18**, pp 183-194 (1998).

4. Armbruster, R. and Mitrovic, J. "Pattern of falling film flow over horizontal smooth tubes", *Proceeding of 10th International Heat Transfer Conference*, **3**, Brighton, UK, pp 275-280 (1994)

5. Chyu, M.C. and Bergles, A.E. "An analytical and experimental study of falling-film evaporation on a horizontal tube", *Transactions of the ASME Journal of Heat Transfer*, **109**, pp 983-990 (1987).

6. Parken, W.H., Fletcher, L.S., Sernas, V. and Han, J.C. "Heat transfer through falling film evaporation and boiling on horizontal tubes", *Transaction of the ASME Heat Transfer*, **112**, pp 744-750 (1990).

7. Fletcher, F. and Sernas, V. "Evaporation from thin water film on horizontal tubes", *Ind. Eng. Chem. Process Des. Dev.*, **13**(3), pp 265-269 (1974).

8. Fletcher, F., Sernas, V. and Parken, H. "Evaporation heat transfer coefficients for thin sea water films on horizontal tubes", *Ind. Eng. Chem. Process Des. Dev.*, **14**(4), pp 411-416 (1975).

9. Lorenz, J.J. and Yang, D. "A note on combined boiling and evaporation of liquid films on horizontal tubes", *ASME Journal of Heat Transfer*, **101**, pp 178-180 (1979).

10. Chen, I.Y. and Kocamustafaogullari, G. "An experimental study and practical correlations for overall heat transfer performance of horizontal tube evaporator design", *Heat Transfer Equipment Fundamentals, Design, Applications and Operating Problems, HTD*, **108**, pp 23-32 (1989).

11. Kocamustafaogullari, G. and Chen, I.Y. "Falling film heat transfer analysis on a bank of horizontal tube evaporator", *AICHE Journal*, **34**(9), pp 1539-1549 (1988).

12. Wang, C.Q., Lu, Z., Li, D.Q., Yu-Chi, B. and Sun, Y.G. "Heat and mass transfer in falling film generator of lithium bromide absorption refrigeration machine", *19th International Congress of Refrigeration 1995, Proceeding*, **IIIa**, pp 209-214 (1995).

13. Kim, D.K. and Kim, M.H. "Heat transfer enhancement characteristics for falling film evaporation on horizontal enhanced tubes with aqueous Li/Br solution", *Enhanced Heat Transfer*, **6**(1), pp 66-69 (1999).